

Four-Dimensional Assimilation of Multitime Wind Profiles over a Single Station and Numerical Simulation of a Mesoscale Convective System Observed during IHOP_2002

LEI ZHANG AND ZHAOXIA PU

Department of Atmospheric Sciences, University of Utah, Salt Lake City, Utah

(Manuscript received 30 July 2010, in final form 23 April 2011)

ABSTRACT

This study examines the impact of assimilating multitime wind profiles over a single station on the numerical simulation of a warm season mesoscale convective system over the region from the Kansas and Oklahoma border to the Texas Panhandle, observed 12–13 June 2002 during the International H₂O Project (IHOP_2002). Wind profile observations, obtained from Goddard Lidar Observatory for Winds (GLOW) are assimilated into an advanced research version of the Weather Research and Forecasting (WRF) model using its four-dimensional variational data assimilation (4DVAR) system. Results indicate that the assimilation of high temporal and vertical resolution GLOW wind profiles has a significant influence on the numerical simulation of the convective initiation and evolution. Besides the wind fields, the structure of the moisture fields associated with the convective system is also improved. Data assimilation has also resulted in a more accurate prediction of the locations and timing of the convection initiations; as a consequence, the skill of quantitative precipitation forecasting is enhanced greatly.

The positive impact of 4DVAR assimilation of multitime wind profiles over a single station on the mesoscale prediction in this study presents a successful procession of the traditional technique in time to space conversion. However, when the data from conventional networks are assimilated into the model with GLOW wind profiles, the data impact is not compatible with that from the assimilation of GLOW wind profiles only, implying the need for a high temporal and spatial resolution wind profile network in order to achieve reasonable mesoscale analysis and forecasting.

1. Introduction

Strong convective storms during the warm season are responsible for a large portion of the annual rainfall over the southern Great Plains (SGP) of the United States. Accurate prediction of quantitative precipitation associated with these warm season systems has been an important task (Fritsch and Carbone 2004). However, although the skill level of numerical weather prediction (NWP) has improved greatly over past two decades, the accurate prediction of the initiation and evolution of mesoscale convective systems (MCS) remains a challenging problem. The prediction of the exact timing, location, and intensity of convective initiations and the subsequent evolution of the convective systems are even more

difficult. Such challenges and difficulties are mostly due to the inadequate understanding and inaccurate representation of the physics processes in the model and the poor specification of atmospheric initial states (Fritsch and Carbone 2004; Wakimoto et al. 2004; Zängl 2004; Zhang et al. 2006). The lack of accurate and high-resolution observations is one of the major obstacles associated with these problems (Stauffer and Seaman 1990).

To address the key processes associated with MCS and the role of the water vapor field in the initiation and evolution of convective systems and their relation to precipitation, the International H₂O Project (IHOP_2002) was conducted during May–June of 2002 (Weckwerth et al. 2004). During the IHOP_2002 field program, numerous research and operational water vapor measuring systems and retrievals, via in situ and remote sensing techniques, were operated in the U.S. southern Great Plains. High-resolution observations of water vapor and atmospheric dynamics were acquired from various instruments (Weckwerth et al. 2008). Previous studies (e.g.,

Corresponding author address: Dr. Zhaoxia Pu, Department of Atmospheric Sciences, University of Utah, 135 S 1460 E, Rm. 819, Salt Lake City, UT 84112.
E-mail: zhaoxia.pu@utah.edu

Childs et al. 2006; Liu and Xue 2008; Wulfmeyer et al. 2006; Xue and Martin 2006) showed that the assimilation of field data resulted in improved numerical simulations of convective initiations and evolutions. Specifically, results from Wulfmeyer et al. (2006) indicated that the assimilation of water vapor differential absorption lidar data improves the simulation of the structures of the moisture field of a convective system.

Although the importance of the high-resolution moisture information in the analysis and simulation of MCS has been well recognized and addressed, and the influence of wind observations, especially the winds in the boundary layers to predicting convection systems, has been recognized for years (Sun and Crook 2001; Crook and Sun 2002; Xiao and Sun 2007), the impact of high-resolution wind measurements, especially the high temporal resolution wind profile measurements, obtained during the IHOP_2002 project on the numerical simulations and predictions of MCS has not been paid much attention. Previous studies indicated that the wind information is one of the critical factors for MCS simulation (LeMone et al. 1998). Studies from Lee et al. (1991) showed that storm initiation is sensitive to the local amount of moisture, strength of convergence, and wind shear values. They also find that the horizontal vorticity in the boundary layer, associated with low-level vertical wind shear, is important for deep convection developments. However, because of the lack of high-resolution wind profile observations before IHOP_2002, fewer studies have been conducted to address the impact of high temporal resolution wind data on the numerical simulations and predictions of mesoscale convective systems.

In view of the available wind profile measurements during IHOP_2002, the objective of this paper is to examine the impact of high temporal and vertical resolution wind profile measurements on the short-range numerical simulations and predictions of MCSs. Specifically, we will evaluate the impact of wind profile measurements obtained from the Goddard Lidar Observatory for Winds (GLOW) on the numerical simulation of warm season convection using an advanced research version of Weather Research and Forecasting (WRF) model (Skamarock et al. 2005) and its four-dimensional variational data assimilation (4DVAR) system (Huang et al. 2009).

The paper is organized as follows. In section 2, the selected convective case and available wind profile measurements are described. Section 3 introduces the WRF model and its 4DVAR data assimilation system. Section 4 presents the details of the model configuration and experimental designs. Numerical results are presented and discussed in section 5. Conclusions are made in section 6.

2. Overview of the convection case

a. Case description

A convective initiation on 12 June 2002 was a major MCS over the IHOP_2002 experimental domain during the field experiment (Weckwerth et al. 2008). It was a complicated case that involves a number of mesoscale systems that interact with each other. During the day of 12 June 2002, a surface low pressure system slowly developed in northwestern Oklahoma. A weak surface cold front extended southward through the Panhandle of Texas and into eastern New Mexico. To the north, along the Kansas and Oklahoma border, an east–west oriented outflow boundary created by convection the previous night remained mostly stationary throughout the day (Liu and Xue 2008; Weckwerth et al. 2008). During the day, a dry-line developed ahead of the surface cold front, just to the east and south of the surface low pressure (Fig. 1). Most of the convections were initiated at about 2100 UTC 12 June 2002 along most of the dryline; isolated convections formed from the Kansas and Oklahoma border to the Texas Panhandle along the dryline (group A in Fig. 2a) and the outflow boundary (group B in Fig. 2a). They then gradually became intense (Fig. 2b). Convections initiated from group A extended northeastward and reached their maximum intensity, and the convections from group B were organized and intensified continuously. At 0100 UTC 13 June (Fig. 2c), group A continued to move southeastward and extended northeastward; after 2 h (0300 UTC 13 June; Fig. 2d) it became weaker and dissipated. At 2300 UTC 12 June (Fig. 2b), group B continued to intensify and extended eastward, as a *squall-line structure was well developed* and an intense convection was formed in the Kansas and Oklahoma border and gradually intensified at 0100 UTC 13 June (Fig. 2c). Afterward, it moved southeastward and organized as a squall line by 0300 UTC 13 June (Fig. 2d) and dissipated after 0900 UTC 13 June 2002. This study focuses on the convective initiations and evolutions as well as the development of the squall-line case during 1800 UTC 12 June to 0300 UTC 13 June.

b. GLOW wind profile observations

GLOW is a mobile direct detection Doppler lidar system (Gentry and Chen 2003). GLOW uses an optical interferometric technique to measure the Doppler shift of the laser signal backscattered by air molecules. The lidar operates at a wavelength of 355 nm and is designed to profile winds in clear air from surface up to the lower stratosphere. In May and June of 2002, GLOW was deployed during IHOP_2002 to collect the continuous time series of wind speed and direction from surface up to the tropopause and to characterize the flow and dynamics in

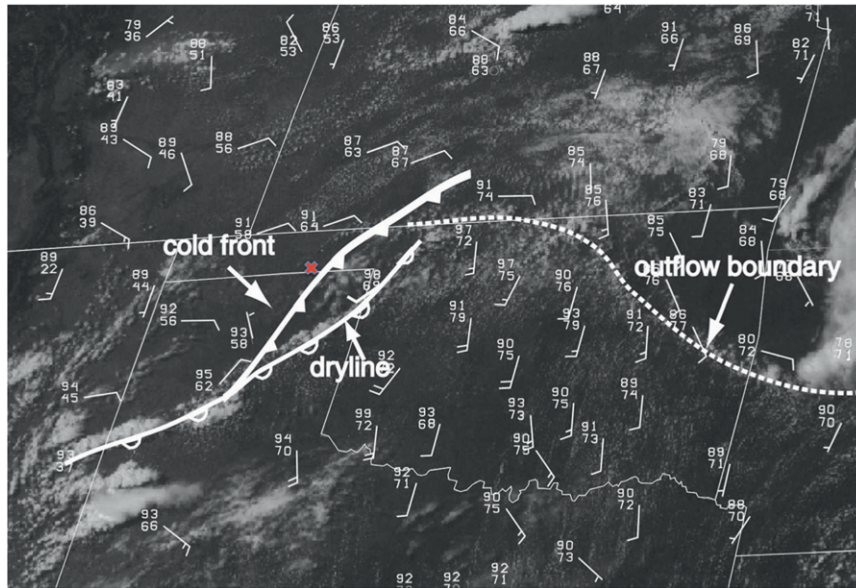


FIG. 1. Visible satellite imagery at 2045 UTC 12 Jun 2002, with surface observations overlaid. Station models show wind barbs (one full barb representing approximately 5 m s^{-1}), and temperature and dewpoint temperature ($^{\circ}\text{F}$) [from Liu and Xue (2008)]. The location of GLOW lidar wind profiling site is marked by a red crisscross.

and above the boundary layer. GLOW is installed at the Homestead profiling site (36.558°N , 100.606°W) in Oklahoma. In addition, several other lidars, radars, and passive instruments are operated from the Homestead site, which provide a unique cluster of observations in the IHOP_2002 field experiments.

During the IHOP_2002, over 240 h of wind profile measurements in 34 operation days were collected with GLOW. After data quality control and preprocessing, there are two types of data products (wind speed, wind direction, and wind u , v component) available: one is in 30-min time intervals and the other is in 10-min time intervals, both with 100-m vertical resolution for altitudes below 3 km and 200-m vertical resolution above 3-km altitudes. Taking advantage of the high temporal resolution, the winds with 10-min intervals are used in the data assimilation experiment in this study. Figure 3 shows the time series of GLOW wind profiles from 1800 to 2100 UTC 12 June 2002 assimilated by 4DVAR in this study. The vertical wind profiles are available from surface up to about 7 km. Almost all of the data profiles passed the default quality control procedure in WRF 4DVAR data assimilation system.

3. Numerical model and data assimilation system

a. WRF model

An Advanced Research version of the WRF model (ARW), developed by the National Center for Atmospheric

Research (NCAR) is used in this study. The ARW is designed to be a flexible, state-of-art atmospheric simulation system. This system is suitable for the use in a wide range of applications across scales from meters to thousands of kilometers such as studies about the physical parameterizations, data assimilation, real-time NWP, etc. A detailed description of the ARW can be found in Skamarock et al. (2005). In this study, a version 3.0.1 of ARW is used in all experiments in this study.

b. 4DVAR system

A 4DVAR data assimilation system is developed by NCAR accompanying the ARW (Huang et al. 2009). It uses the incremental 4DVAR formulations that are commonly used in operational systems (Courtier et al. 1994; Veerse and Thépaut 1998; Lorenc 2003). The increment approach is designed to find the optimal analysis increments by minimizing a predefined cost function that is defined as a function of the analysis increment instead of analysis itself (Huang et al. 2009). Unlike the three-dimensional variational data assimilation (3DVAR) method, the 4DVAR assimilates observations continuously within an assimilation time window instead of assimilating observations only once at the analysis time. This is particularly important in the regions with high temporal and spatial variability during severe weather events. In addition, since the continuous data assimilation technique uses the model as a constraint to impose the dynamic balance on the assimilation, therefore, in principle, it is

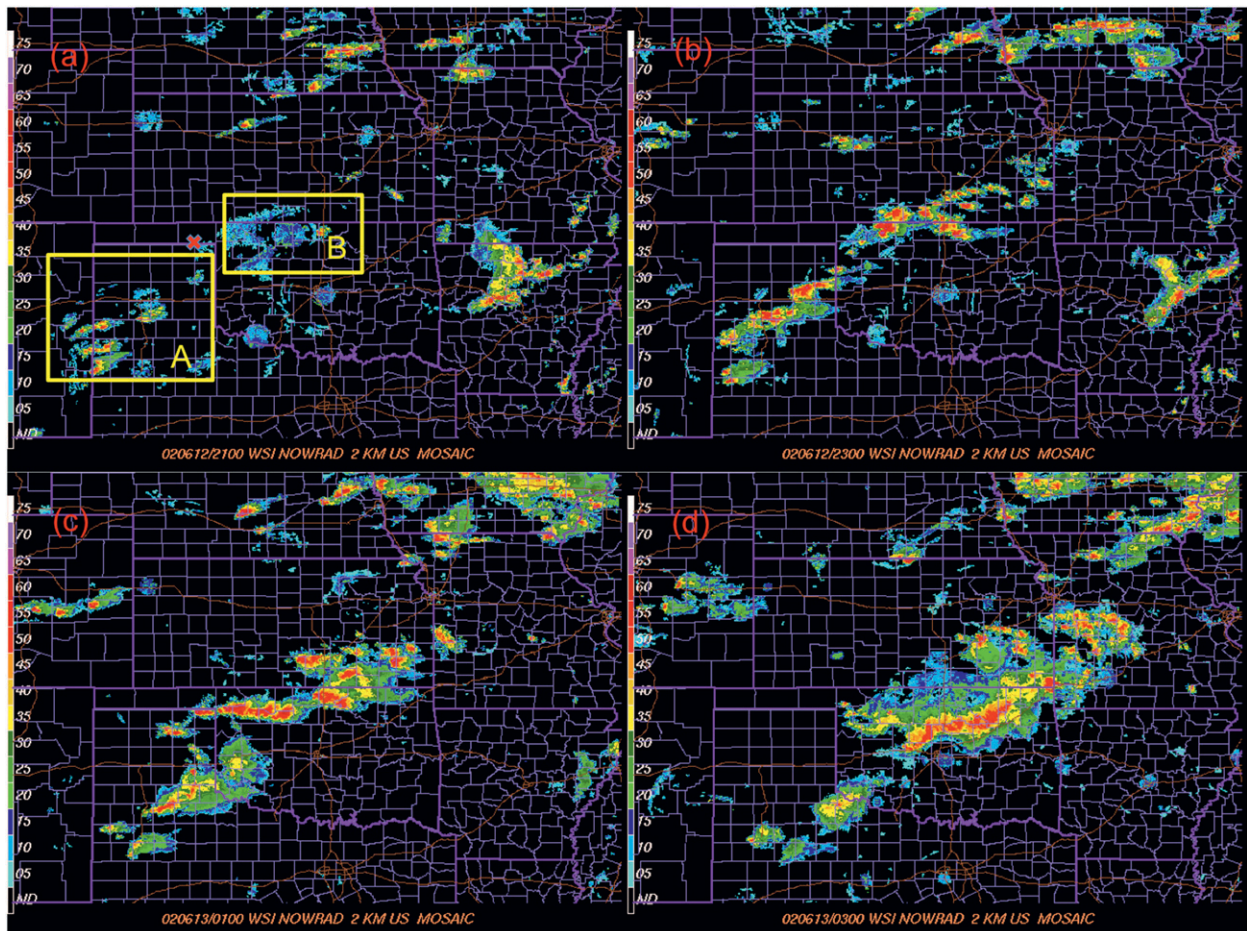


FIG. 2. Composite radar reflectivity observations at (a) 2100 UTC 12 Jun 2002, (b) 2300 UTC 12 Jun 2002, (c) 0100 UTC 13 Jun 2002, and (d) 0300 UTC 13 Jun 2002. The location of GLOW lidar wind profiling site is marked by a red crisscross in (a). (Data are from WSI IHOP 2002 2-km resolution sector mosaic reflectivity imagery dataset.)

expected to perform better than 3DVAR, although it is computationally expensive.

In this study, the first-guess field (background field) is generated by a 6-h WRF model forecast started at 1200 UTC 12 June 2002. Following Huang et al. (2009), the background error covariance matrix \mathbf{B} is generated with the National Meteorological Center [NMC; now known as National Centers for Environmental Prediction (NCEP)] method (Parrish and Derber 1992; Barker et al. 2004) over the model domain. Horizontally isotropic and homogeneous recursive filters are applied to horizontal components of background error. Since we generated \mathbf{B} specifically over the model domain, the horizontal length scale for the recursive filter is set to 1.0 in all data assimilation experiments. In vertical direction, the observation information is spread by the empirical orthogonal function (EOF) technique. The vertical component of background error is projected onto a climatologically averaged (in time, longitude, and latitude) eigenvector of vertical error

estimated with the NMC method. Because the winds are model variables, the observation operator is a simple interpolator in space. The observational error covariance matrix for GLOW wind data is treated as a diagonal matrix with statistically determined variances of $4 \text{ m}^2 \text{ s}^{-2}$. According to the observational data availability, the assimilation time window is set to 3 h between 1800 and 2100 UTC 12 June 2002.

4. Experimental design

a. WRF model configurations

A two-way nested interactive simulation is conducted in this study. The model horizontal spacing is 9 km for the outer domain and 3 km for the inner domain. Sizes of model grids are 237×187 and 394×307 for the outer and inner domains, respectively. Figure 4 shows the model domain used in all experiments. The location of the GLOW lidar wind-profiling site is also marked. There are

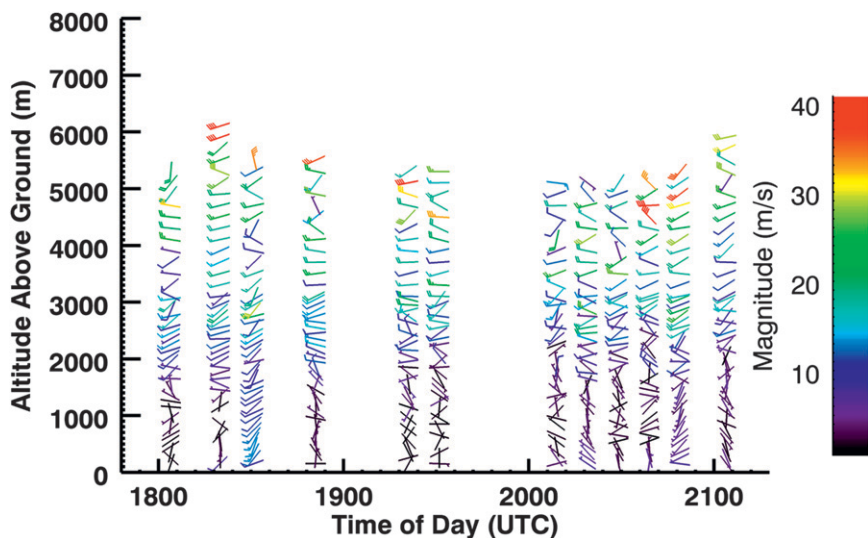


FIG. 3. Time series of GLOW wind profiles at Homestead profiling site (36.558°N , 100.606°W) from 1800 to 2100 UTC Jun 2002. Colors represent the different magnitudes of wind speeds.

a total of 38 vertical model levels from the surface up to 50 hPa. ARW offers multiple options for various physical parameterization schemes. In this study, the model physical options include the Purdue–Lin microphysics scheme (Chen and Sun 2002), the Yonsei University (YSU) planetary boundary layer scheme (Hong and Pan 1996), the Kain–Fritsch cumulus parameterization scheme (Kain and Fritsch 1993), the Noah land surface model (Chen and Dudhia 2001), the Rapid Radiative Transfer Model (RRTM; Mlawer et al. 1997) longwave, and the Dudhia shortwave radiation scheme (Dudhia 1989). The cumulus parameterization scheme is only applied to 9-km grid domain.

The analysis from Eta Data Assimilation System (EDAS) on the Advanced Weather and Interactive Processing System (AWIP) grids 212 archived by NCEP is used to provide boundary conditions for numerical simulations. The NCEP AWIP dataset is available at 3-h intervals with a horizontal resolution of about 40 km over the North America.

Instead of directly using the NCEP AWIP analysis for the first guess in the 4DVAR experiment, an ARW simulation initialized by the WRF standard initialization process package using the NCEP AWIP analysis, was first integrated 6 h from 1200 to 1800 UTC 12 June 2002 to provide a first-guess field for the 4DVAR experiment. The control experiment continued without additional data assimilated.

b. Experimental design

Four experiments are conducted: the first one is a “control” simulation without data assimilation, the second

one assimilates GLOW wind profiles using 4DVAR, the third one assimilates conventional data (surface and radiosonde observations), and the last one assimilates both GLOW wind profiles and the conventional observations. In all data assimilation experiments, the GLOW lidar wind profiles (u and v components at various heights) are assimilated every 10 min, while the surface and radiosonde data are assimilated hourly. Table 1 lists the details of these four experiments. The assimilation time window is set from 1800 to 2100 UTC 12 June 2002, near the time of the observed convective initiation. The observation error for GLOW wind profiles is set to 2 m s^{-1} . The data

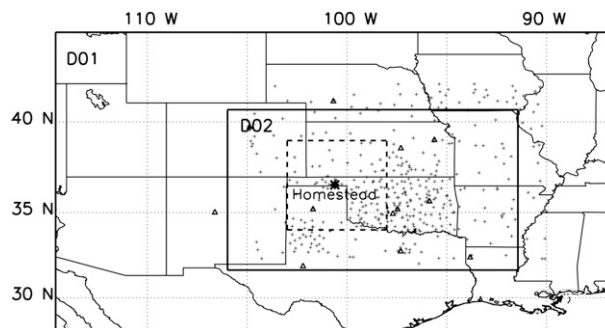


FIG. 4. Locations of the model domains (D01 and D02) and the distributions of observations at 1800 UTC 12 Jun 2002. The outer domain (D01) has 9-km horizontal resolution; the inner domain (D02) has 3-km horizontal resolution. The Homestead GLOW lidar wind profiling site is marked by an asterisk, the stations of the conventional surface observations are marked by plus signs, and the conventional radiosonde profile measurements are marked by triangles. The square box marked by the dashed lines indicates the region used in the statistics in Fig. 16.

TABLE 1. Details of the experimental designs.

Name of expt	Assimilated observation type	Observation frequency
CTRL	—	—
4DVAR	Lidar wind profiles	10 min
CONV	Surface and radiosonde data	Hourly
BOTH	Lidar wind profiles	10 min
	Surface and radiosonde data	Hourly

assimilation is performed on the 9-km resolution domain. The 3-km grids are initialized by interpolating the variables from these in the 9-km domain after the data assimilation. Then, the model is integrated for both domains for a 12-h forecast from 1800 UTC 12 June to 0600 UTC 13 June 2002. In all data assimilation experiments, a simple data quality control is conducted: if the difference between the observation and the background field (first guess) is larger than 5 times of the observational error, the observation is removed before data assimilation. All results presented in this paper are from simulations at the 3-km domain. For simplification, four experiments (as listed in Table 1) are hereafter referred as “CTRL,” “4DVAR,” “CONV,” and “BOTH,” respectively.

5. Experimental results

a. Impact of GLOW data on analysis fields: CTRL versus 4DVAR

1) ANALYSIS INCREMENTS

Figure 5 shows the analysis increments as the differences between CTRL and 4DVAR of u and v components of winds, temperature, and water vapor mixing ratio at 850-hPa pressure level at the end of the data assimilation (2100 UTC 12 June 2002). Large differences are found in the regions along the dryline. For wind and temperature fields, the large differences between CTRL and 4DVAR are mainly in the northwest corner of the Oklahoma and Texas border. The wind fields are strengthened over most of the model domain, especially around the Texas Panhandle area, while in the Texas and Oklahoma border region, weaker winds are found in the 4DVAR experiment. After data assimilation, large temperature increases (Fig. 5c) are produced in the northwest corner of Texas and the Texas and Oklahoma border areas. In these regions, the temperature is increased up to 3.0 K. A large moisture increase is found near the southwestern corner of Kansas and the western corner of Oklahoma and Texas border, while the large moisture decrease appears in the northwest of Oklahoma. In the Kansas and Texas border, the water vapor mixing ratio increases up to 1.0 g kg^{-1} . Up to

2.5 g kg^{-1} of increases are found in the northwest corner of the Texas and Oklahoma border, while in northwest Oklahoma the water vapor mixing ratio decreases by 2.0 g kg^{-1} . Therefore, the moisture gradient over the Texas and Oklahoma northwest border region is reduced after the data assimilation. In the area where the real initiation took place (near the Texas Panhandle area), the moisture gradient is increased, implying a favorable condition for the convective initiation.

2) WIND FIELDS

Figure 6 demonstrates the histogram of the wind departures of observations from first guess winds ($O - B$) and analysis winds ($O - A$) for u and v components at the Homestead profiling site (36.558°N , 100.606°W) in 4DVAR experiment during the 3-h assimilation period (between 1800 and 2100 UTC 12 June 2002). Results show that 4DVAR is effective in drawing the analysis close to the observations. The mean departures are reduced significantly. For the wind u component, the mean departure is reduced from 0.6945 to 0.0586 m s^{-1} , for the wind v component, the mean departure is reduced from 1.0639 to 0.1628 m s^{-1} . In the meantime, the root-mean-square errors (RMSE) are also reduced. The RMSE of the u component is reduced from 4.0555 to 3.1238 m s^{-1} , and the RMSE of the v component is reduced from 3.9948 to 3.2334 m s^{-1} . The correlation coefficients are also computed for the two experiments (CTRL and 4DVAR). Statistical results show that the correlation coefficients of wind between observations and background (CTRL) for u , v components during the whole period are 0.85 and 0.45, respectively. After data assimilation, the correlation coefficients between observations and analysis (4DVAR) increase to 0.91 and 0.58 for the u and v components of wind, respectively.

Figures 7a and 7e compare the horizontal wind fields at 850 hPa at 2100 UTC 12 June 2002 (the end of the data assimilation) in CTRL (Fig. 7a) and 4DVAR (Fig. 7e). The shaded areas indicate the regions with horizontal wind speeds exceeding 10 m s^{-1} . It is apparent that major differences between CTRL and 4DVAR occur mainly in the region where the convection initiation takes place. After data assimilation (Fig. 7e), the winds in northwest Oklahoma and Texas border are weakened, while the wind fields in the northeast of Texas Panhandle are strengthened. In 4DVAR, a strong wind shift appears along the dryline (Fig. 7e). More importantly, significant differences in vertical velocity fields are found between CTRL and 4DVAR (Figs. 8a,e) along with contour lines of the temperature field. Clearly, the locations of maximum vertical velocity are different before and after data assimilation. Compared with the observed location of convection initiations (Fig. 2a), the CTRL experiment

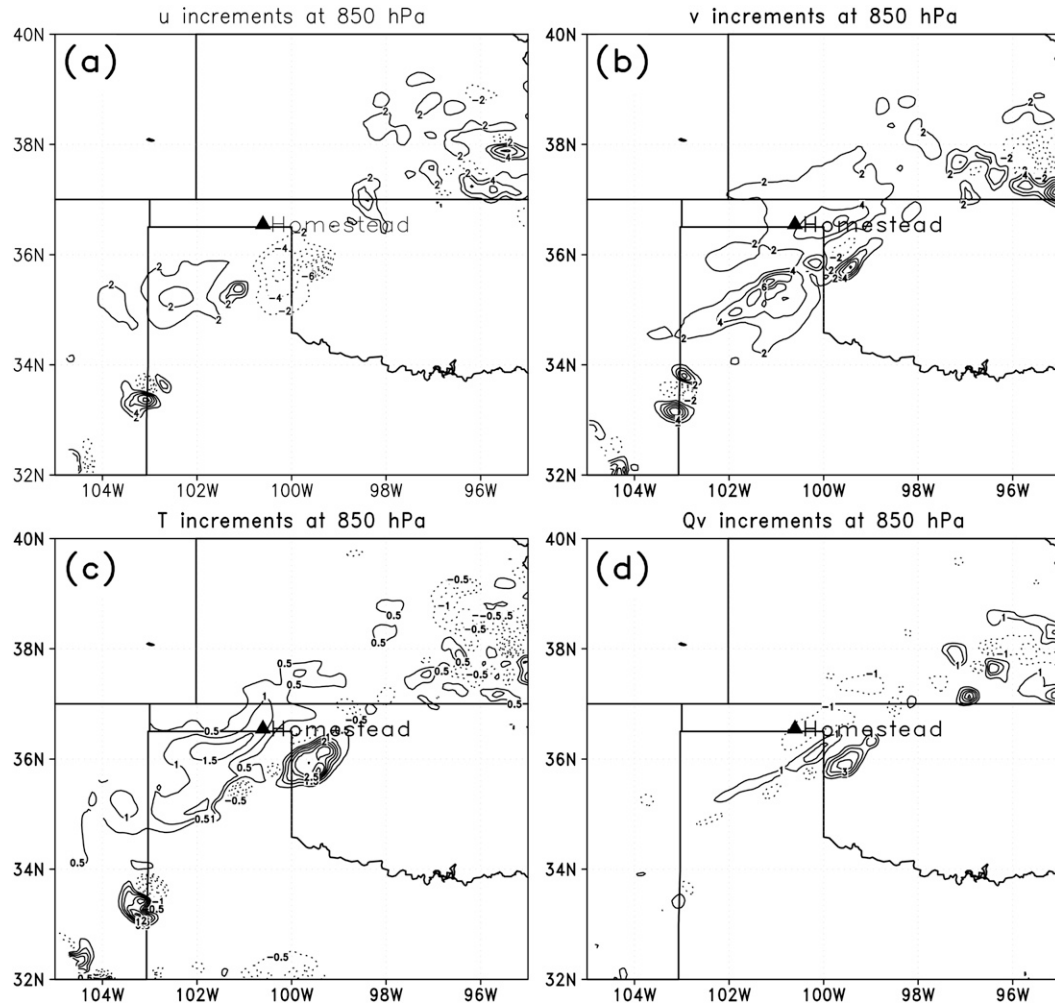


FIG. 5. Analysis increments as the differences between the control and 4DVAR experiments for (a) u component (unit: m s^{-1} , contour interval: 2 m s^{-1}), (b) v component (unit: m s^{-1} , contour interval: 2 m s^{-1}), (c) temperature (unit: K, contour interval: 0.5 K), and (d) water vapor mixing ratio (unit: g kg^{-1} , contour interval: 1 g kg^{-1}) at 850 hPa at 2100 UTC 12 Jun 2002. The Homestead GLOW lidar profiling site is marked by a closed triangle. The solid (dashed) lines represent the positive (negative) values.

overestimated the convective regions in the northwest Oklahoma and Texas border and underestimated the convective elements near the Texas Panhandle. The simulated locations of the convection (Fig. 8a) in CTRL are further northeast than the observed locations, whereas the locations of the convection initiation in the 4DVAR experiment (Fig. 8e) are much closer to the locations of the observed convective initiations. The simulated horizontal and vertical wind fields in 4DVAR are corresponding with the split of two convective cells (Figs. 7e and 8e).

Fortunately, there are unmanned Doppler radar wind profile observations available from one of the stations [named VCIO2, located at (36.07°N , 99.21°W)] in the National Oceanic and Atmospheric Administration (NOAA)

Profiler Network (NPN, see online at <http://www.profiler.noaa.gov/npn/index.jsp>) near the key area of the analysis differences between CTRL and 4DVAR. To verify the realistic of wind profiles in numerical simulations, differences between the hourly wind profiles generated by CTRL/4DVAR and measured by NPN profiler are calculated for the period of 2100 UTC 12 June–0300 UTC 13 June 2002. Figure 9 illustrates the vertical distribution of the time-averaged RMSE of wind speed and direction from CTRL and 4DVAR against the wind profile measurements over the VCIO2 site. It is clear that the wind fields are improved in 4DVAR over the area during the whole period of numerical simulation, indicating the improvement in the initial wind fields by 4DVAR.

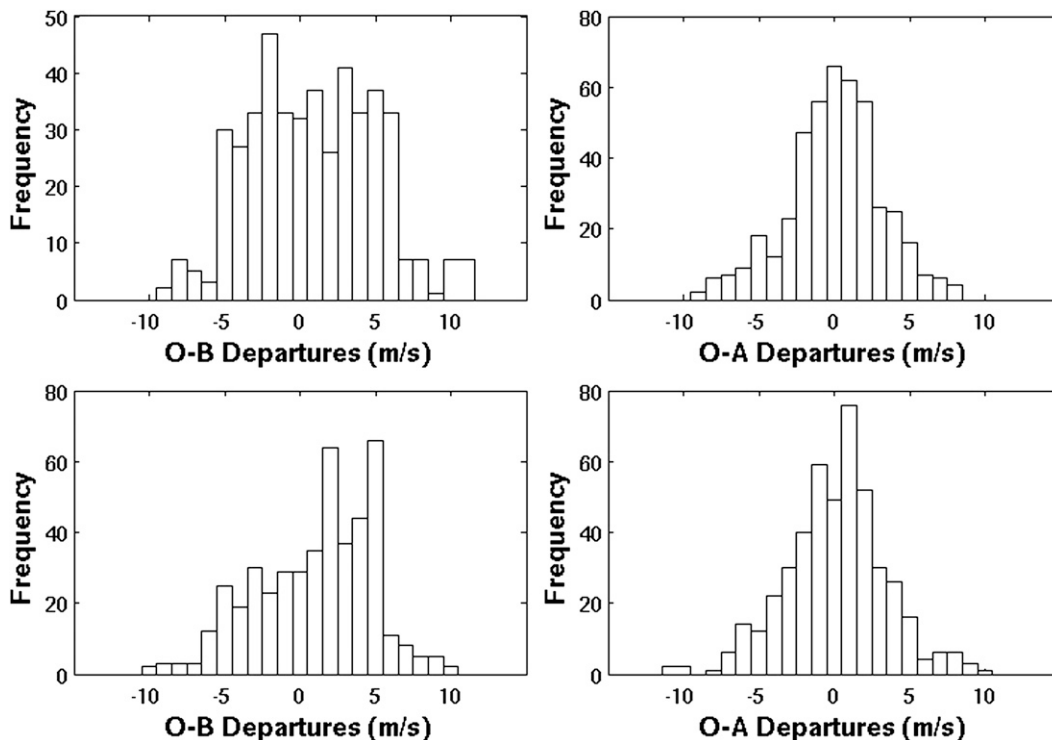


FIG. 6. Histograms of wind departures of lidar wind observations from (left) first-guess winds ($O - B$) and (right) analysis winds ($O - A$) for (top) wind u components and (bottom) wind v component from experiment 4DVAR.

3) MOISTURE FIELDS

Figure 10 illustrates the model-simulated water vapor mixing ratio, moisture convergence, and vertical vorticity fields near the surface at 2100 UTC 12 June 2002. It shows that the assimilation of GLOW high-resolution wind profiles has resulted in a redistribution of the model moisture fields. The simulated locations of convergence from CTRL and 4DVAR are different. In CTRL, the convection mainly occurs in northwest Texas and near the Oklahoma border along the dryline, where large moisture gradients are produced (Figs. 10a,c). In 4DVAR, the convections are mainly presented in the Texas Panhandle region (Figs. 10b,d). Moisture fields in the Texas Panhandle and the northwestern corner of the Oklahoma border become dryer, while in the regions northeast of the Panhandle along the dryline are wetted after data assimilation (Fig. 10d). This agrees well with the model-simulated 850-hPa reflectivity distributions (Figs. 11a,e). Comparing the simulated radar reflectivity (Figs. 11a,e) with radar observations (Fig. 2a), the 4DVAR experiment also produces a more realistic simulation of the convection initiation (Fig. 11e).

It should be noted from the above results that, although only wind profiles from a single station were assimilated

into the WRF model using its 4DVAR system, the analysis increments (Fig. 5) during the data assimilation show a reasonable spatial distribution. The multitime observations at a single station influenced the spatial distribution of the state variables. More importantly, since the numerical model itself was used in 4DVAR as a strong constraint, even though only wind information was assimilated, the temperature and moisture fields were also adjusted.

b. Impact of GLOW data on forecasts: CTRL versus 4DVAR

1) WIND FIELDS

Figure 7 shows the horizontal wind fields at 850 hPa at 4 simulation times (2100 UTC 12 June, 2300 UTC 12 June, 0100 UTC 13 June, and 0300 UTC 13 June 2002). As mentioned, at 2100 UTC (Figs. 7a,e) both CTRL and 4DVAR produce an unrealistic convection in the Oklahoma and Kansas border. In CTRL, the convections along the dryline are initiated in northwest Oklahoma and Texas border, which is farther north and east of the observed convection initiations (Fig. 2a). Owing to the different locations of the convective initiation in these two experiments, the evolutions of the MCS simulated from CTRL and 4DVAR experiment are also different. Two hours

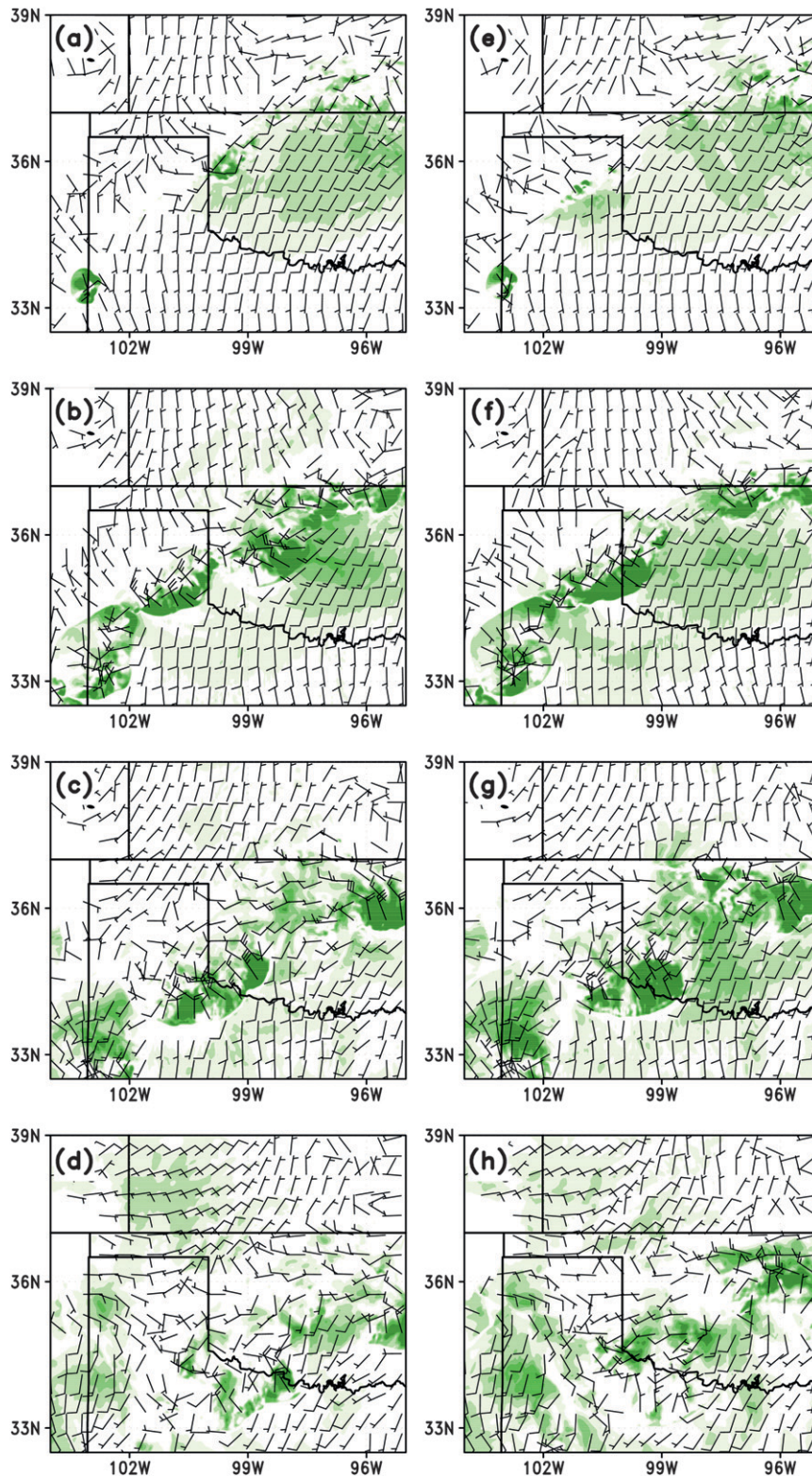


FIG. 7. Simulated horizontal winds (m s^{-1}) at 850 hPa from (a)–(d) control and (e)–(h) 4DVAR experiments at (a),(e) 2100 UTC 12 Jun 2002; (b),(f) 2300 UTC 12 Jun 2002; (c),(g) 0100 UTC 13 Jun 2002; and (d),(h) 0300 UTC 13 Jun 2002. Shaded contours indicate the areas with wind speed exceeding 10 m s^{-1} .

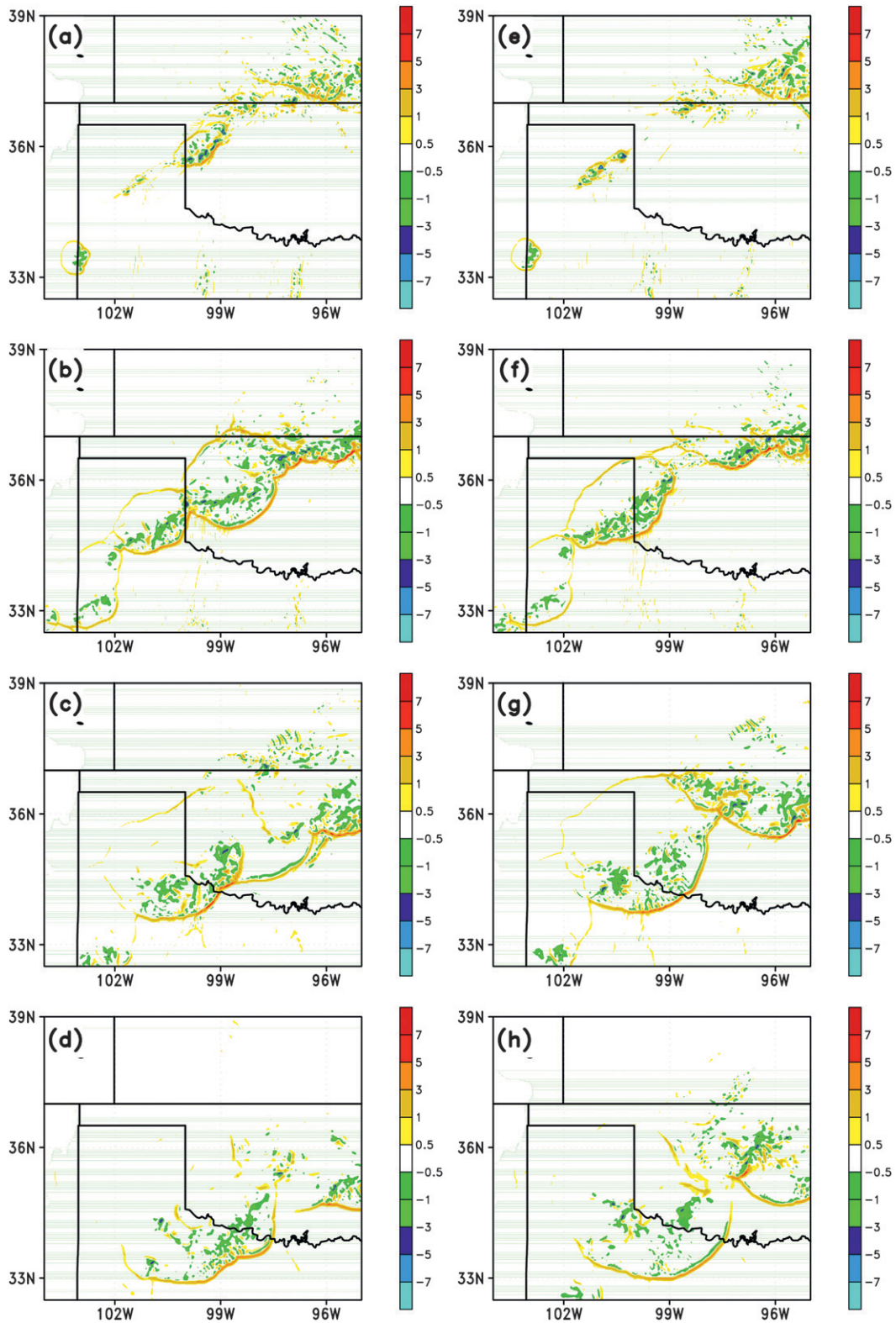


FIG. 8. Simulated vertical velocity (m s^{-1}) at 850 hPa from (a)–(d) control and (e)–(h) 4DVAR experiments at (a),(e) 2100 UTC 12 Jun 2002; (b),(f) 2300 UTC 12 Jun 2002; (c),(g) 0100 UTC 13 Jun 2002; (d),(h) 0300 UTC 13 Jun 2002.

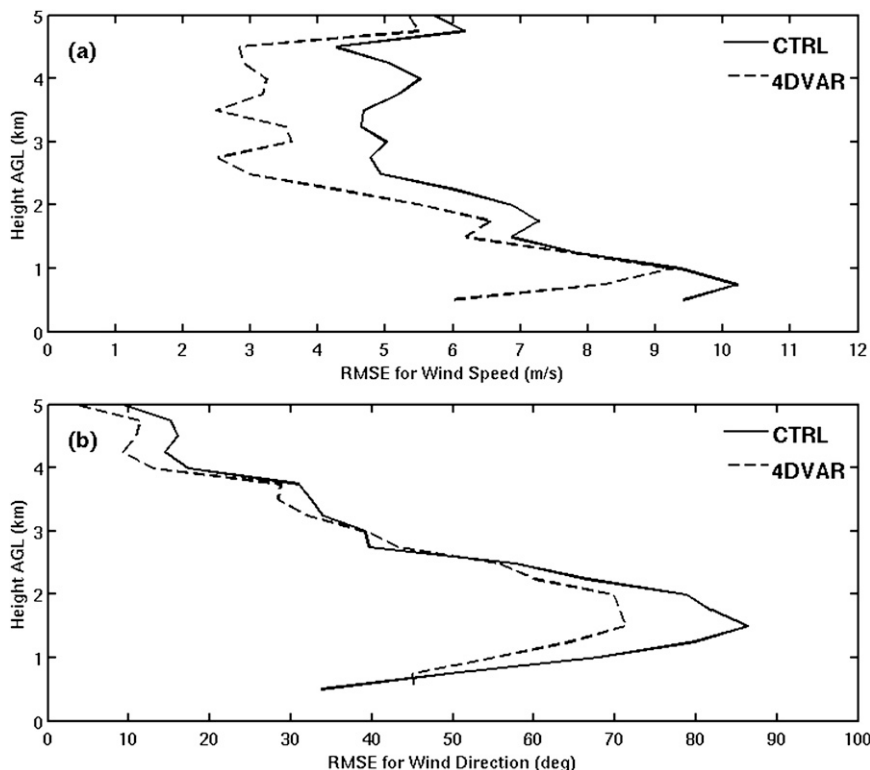


FIG. 9. Vertical distribution of the RMSE of wind (a) speed and (b) direction for CTRL and 4DVAR against the Doppler radar wind profile measurements over the NPN profiler site at (36.07°N, 99.21°W). The RMSE is averaged over the period of 2100 UTC 12 Jun–0300 UTC 13 Jun 2002.

later (at 2300 UTC 12 June; Figs. 7b,f), the differences between these two experiments become more obvious. In CTRL, the convections along the dryline continue to move southeastward and extend eastward. The wind fields in northwest Oklahoma are continuously intensified; in 4DVAR, the convections also move southeastward and intensify gradually, but the locations of the intensification are different from CTRL. The wind fields are mainly intensified in northwest Oklahoma and near the Texas border and also along the Kansas–Oklahoma border. The horizontal winds in the outflow boundary region are intensified. At 0100 UTC 13 June (Figs. 7c,g), the simulated convections in the Oklahoma and Kansas border are intensified further in 4DVAR experiment, whereas CTRL experiment fails to predict these events. At 0300 UTC 13 June (Figs. 7d,h) the convections initiated from the outflow boundary region (group B) in north Oklahoma are still visible in 4DVAR, while they have already been dissipated in CTRL.

Figure 8 presents the vertical velocity at 850 hPa at different times (the same time as showed in Fig. 7). Similar to what have been found in the horizontal wind simulations, the locations of convective initiations in 4DVAR

correspond more with the observations (Fig. 2) than those in CTRL. In particular, the simulated convections initiated over the Kansas and Oklahoma border (associated with a squall line) intensify rapidly in CTRL during the first 4 h of simulation, after that, they dissipate quickly. At 0300 UTC, they have disappeared completely (Fig. 8d). In 4DVAR, the convections are well simulated during the 6-h simulation (Fig. 8h) compared against the observations (Fig. 2). The time evolution and location of the squall-line development over the Kansas and Oklahoma border region are well depicted.

2) REFLECTIVITY FIELDS

Radar reflectivity is heavily related to the variation of hydrometer fields. The simulated composite radar reflectivity from CTRL and 4DVAR at different forecast times (corresponding to Fig. 8) are presented in Fig. 11. Compared with the reflectivities in CTRL (Figs. 11a–d), the time evolutions of model predicted reflectivity patterns in 4DVAR (Figs. 11e–h) are much closer to those from radar observations (Figs. 2a–d). Specifically, at 2100 UTC 12 June, in CTRL (Fig. 11a), a southwest–northeast-oriented area of convection along the dryline is

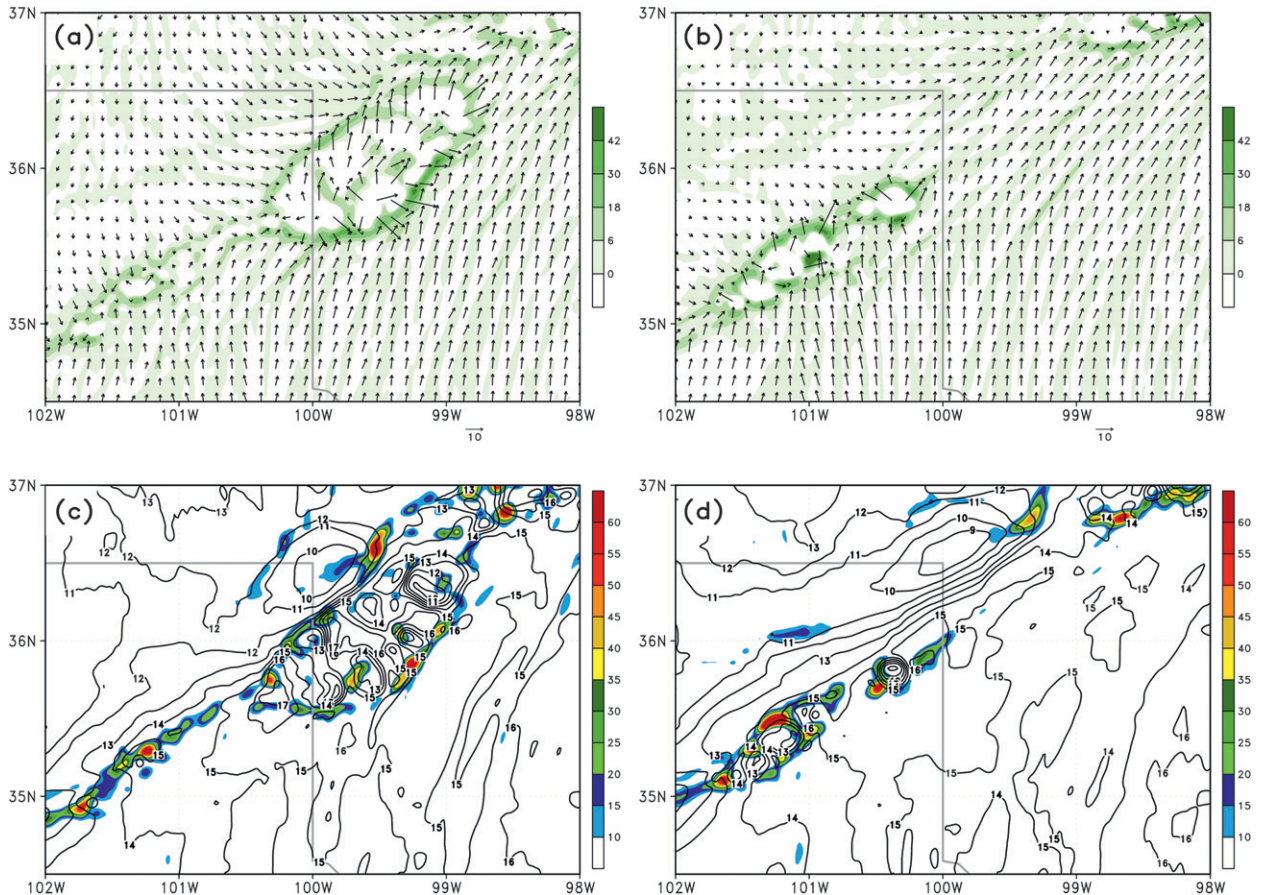


FIG. 10. Model-simulated moisture convergence fields (shaded contour; values of color shading amplified by a factor of 1000) and the horizontal wind vectors (m s^{-1}) near the surface at 2100 UTC 12 Jun 2002 from (a) control and (b) 4DVAR experiments; (c), (d) the water vapor mixing ratio (contour in black, g kg^{-1}) and the vertical vorticity (color shading, amplified by a factor of 10^5) near the surface at 2100 UTC 12 Jun 2002 from (c) control and (d) 4DVAR experiments.

initiated on the Texas and Oklahoma border and it mainly occurs in the Oklahoma region. Compared with radar observed convection, particularly the group A in Fig. 2a, the location of convection initiations is well simulated in 4DVAR. Two hours later (at 2300 UTC 12 June 2002; Figs. 11b,f), in both CTRL and 4DVAR, convections initiated from both group A and B are gradually intensified and continue moving southeastward. But, compared to the radar observations (Fig. 2b), the intensity of the convection is overestimated in northwest Oklahoma in CTRL. The convection that initiated from group A is underestimated northwest of the Texas and Oklahoma border. Meanwhile, the predicted reflectivity distribution in 4DVAR is more realistic compared to CTRL simulation. At 0100 UTC 13 June (Figs. 11c,g), in CTRL, convections initiated from group A splits into two isolated parts, while the convections initiated from group B continues to move eastward and becomes weak. In 4DVAR, convection group A also weakens, while group B

continues to intensify and extends westward and moves southeastward. A squall-line structure is well represented. Comparing CTRL with 4DVAR, large differences are found in the Oklahoma and Texas border areas. In CTRL, no convections are predicted, whereas the 4DVAR experiment successfully predicts the squall-line structures over those regions although the predicted convections are weaker than these in radar observations. At 0300 UTC 13 June (Figs. 11d,h), in both CTRL and 4DVAR, convections initiated from group A continue to weaken and disappear after a few hours. Compared with radar observations (Fig. 2), 4DVAR produces more realistic evolution of convection systems. For the convective areas initiated from group B, at 0300 UTC 13 June they have dissipated and become almost invisible in CTRL, while the convective areas are still clearly visible in 4DVAR although the predicted convection intensity is weaker than that from radar observations. Similar to the moisture fields, large differences are also found in

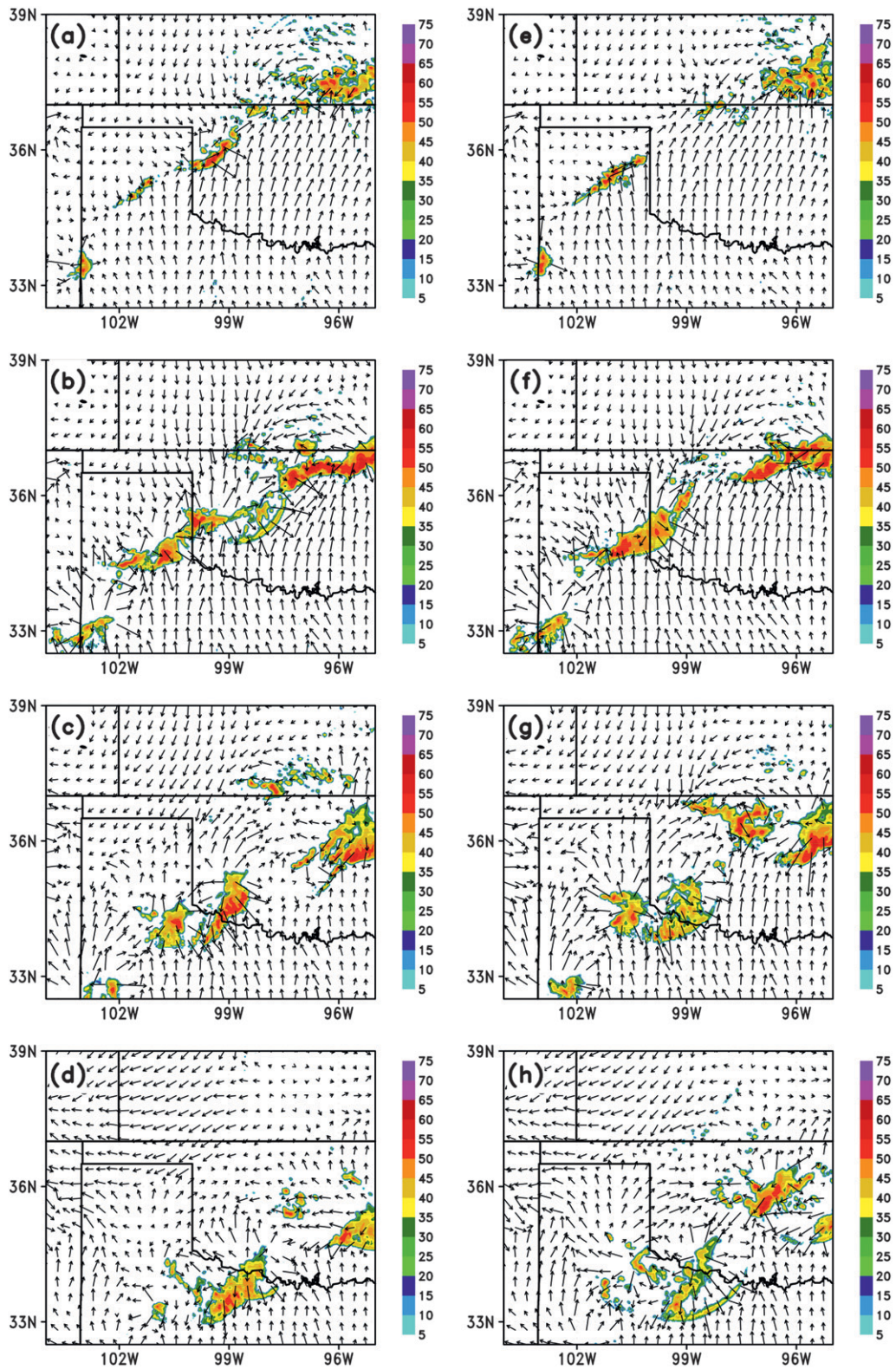


FIG. 11. Simulated surface wind vectors and composite radar reflectivity (dbZ, shaded contours) from (a)–(d) control and (e)–(h) 4DVAR experiments at (a),(e) 2100 UTC 12 Jun 2002; (b),(f) 2300 UTC 12 Jun 2002; (c),(g) 0100 UTC 13 Jun 2002; and (d),(h) 0300 UTC 13 Jun 2002.

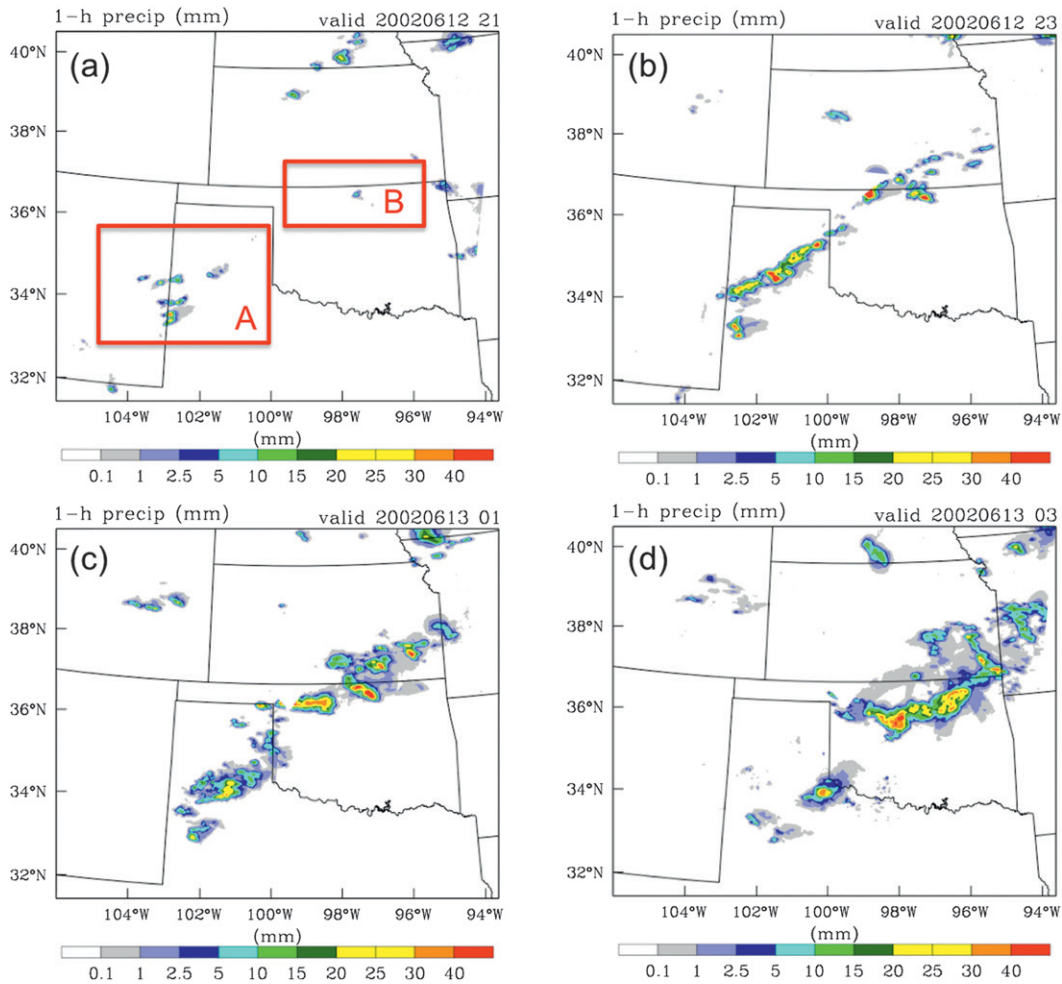


FIG. 12. Observed accumulated 1-h precipitation (mm) from NCEP stage-IV dataset at (a) 2100 UTC 12 Jun 2002, (b) 2300 UTC 12 Jun 2002, (c) 0100 UTC 13 Jun 2002, and (d) 0300 UTC 13 Jun 2002. In (a), the rectangles A and B correspond to the same regions A and B marked in Fig. 2a, respectively.

temperature field (not shown) between the CTRL and 4DVAR experiments.

3) PRECIPITATION FORECASTS

For the convective systems studied in this paper, the main concern is the precipitation over the Texas–Oklahoma–Kansas region between 2100 UTC 12 June and 0300 UTC 13 June 2002. Figure 12 shows the observed accumulated hourly precipitation from NCEP stage-IV rainfall dataset. The regions marked with “A” and “B” in Fig. 12a correspond to the same regions marked in Fig. 2a. At 2100 UTC 12 June (Fig. 12a). The precipitation areas are mainly located in the western border of Texas (region A); they then become intense and extend northeastward to form a northeast–southwest-oriented rainband (at 2300 UTC 12 June; Fig. 12b). After that it continues to move southeastward, and the precipitation in Texas is

weakened while the precipitation in the Oklahoma and Kansas border is intensified further at 0100 UTC 13 June (Fig. 12c) and at 0300 UTC 13 June (Fig. 12d).

Figure 13 presents the precipitation forecasts in CTRL and 4DVAR at four corresponding times. Compared with the observations (Fig. 12), both locations and the amount of the precipitation are better predicted in 4DVAR than that in CTRL. At 2100 UTC 12 June (Figs. 12a,e), both CTRL and 4DVAR predict too much precipitation in the Kansas and Oklahoma border area, compared with group B in Fig. 12a. Corresponding to group A, shown in Fig. 12a, CTRL produces the predicted precipitation at the location that is farther north and east of observed locations (Fig. 13a) while 4DVAR (Fig. 13e) produces a more accurate precipitation forecast. Two hours later (at 2300 UTC 12 June; Figs. 13b,f), the differences between CTRL and 4DVAR become more obvious. For

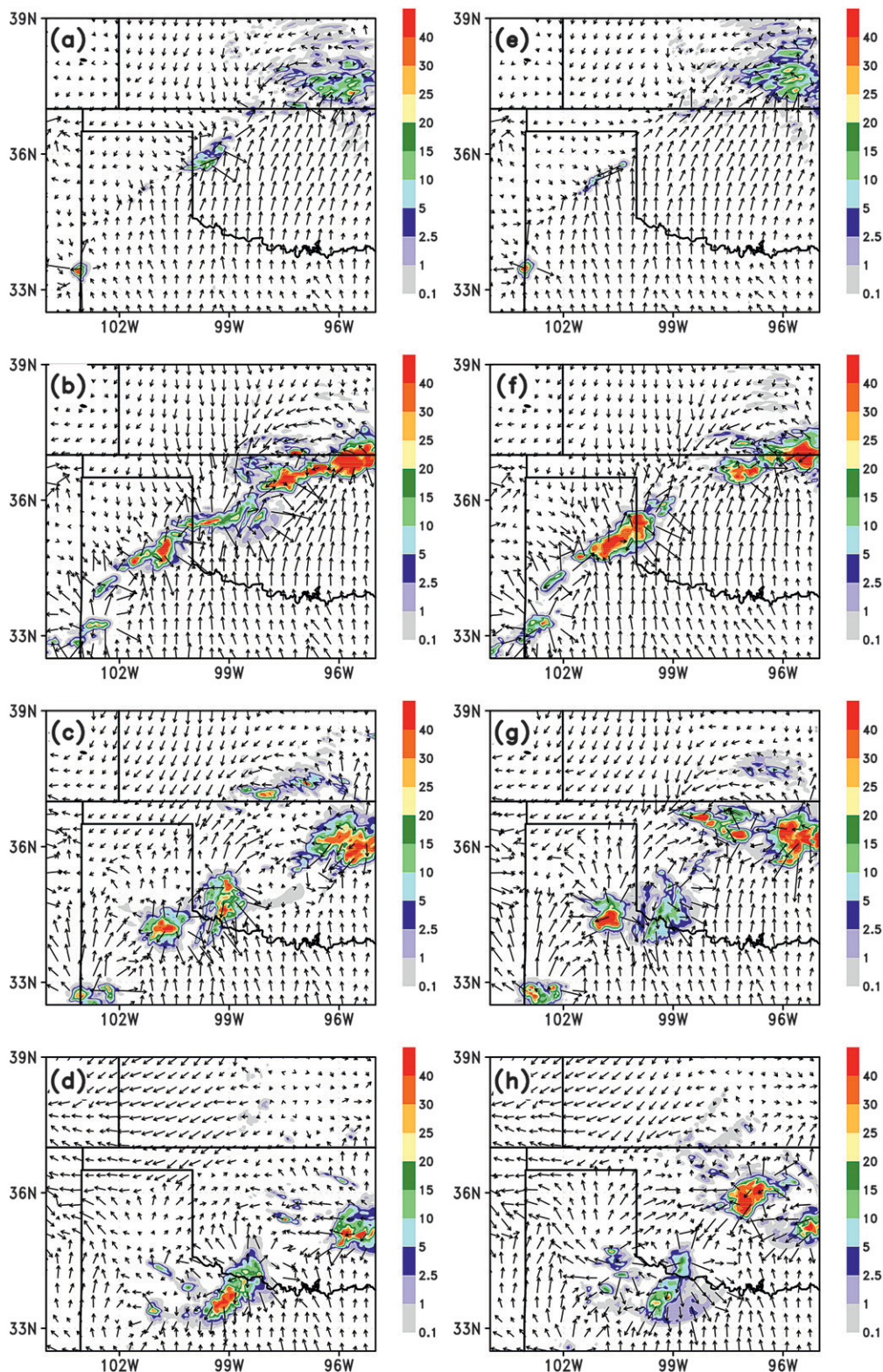


FIG. 13. Simulated surface wind vectors and accumulated 1-h precipitation (mm, shaded contours) from (a)–(d) control run and (e)–(h) 4DVAR data assimilation experiment at (a),(e) 2100 UTC 12 Jun 2002; (b),(f) 2300 UTC 12 Jun 2002; (c),(g) 0100 UTC 13 Jun 2002; and (d),(h) 0300 UTC 13 Jun 2002.

convection group A, 4DVAR produces a more intensive precipitation forecast compared to the CTRL forecast. At 0100 UTC (Figs. 13c,g), large differences between CTRL and 4DVAR are found in the Kansas and Oklahoma border. Compared with the observations (Fig. 12c), 4DVAR makes a more accurate precipitation forecast than CTRL. At 0300 UTC 13 June (Figs. 12d,h), CTRL fails to predict the precipitation event in the northwest of Oklahoma, but 4DVAR predicts this event successfully although the predicted rainfall amount and area are smaller than those from NCEP observations.

To further examine the impact of assimilating wind profiles on the precipitation forecast, the quantitative precipitation forecast (QPF) skill is evaluated for both CTRL and 4DVAR. The verification scores used in this study are derived from a contingency table approach (Wilks 1995). The equitable threat scores (ETS) are computed using the following equation:

$$\text{ETS} = \frac{A}{A + B + C}. \quad (1)$$

For a given threshold, A represents the number of grid points that the model forecast and observation exceed the threshold; B denotes the number of grid points that the model forecast exceeds the threshold, but the observation does not; and C is the number of grid points when the model forecast does not reach the threshold, but the observation exceeds it.

To evaluate the relative skill between 4DVAR and CTRL experiments, we define the following index for the comparison:

$$R = \frac{\text{ETS}_{4\text{dvar}}}{\text{ETS}_{\text{ctrl}}}, \quad (2)$$

where R is the ratio of threat scores between 4DVAR and CTRL; and ETS_{ctrl} and $\text{ETS}_{4\text{dvar}}$ are threat score from CTRL and 4DVAR, respectively. In the case, when R greater than 1, the QPF skill is improved by 4DVAR.

Figure 14 presents the values of R for the hourly rainfall at different times for a domain of (33.5°–37.5°N, 103.0°–96.0°W), the main areas over which the convective systems occurred. Precipitation verification is performed using NCEP stage-IV hourly rainfall dataset with different thresholds: 0.1, 0.25, 0.5, 1.0, 2.5 and 5.0 mm. In general, the assimilation of wind profiles has a positive impact on QPF skill. The ETS scores are higher in 4DVAR at most forecast times. Specifically, the ETS scores of small rainfall (<1.0 mm) at 2100 UTC 12 June are improved significantly. The scores of heavy rainfall (≥ 5.0 mm) at 0100 and 0300 UTC 13 June 2002 are also increased greatly.

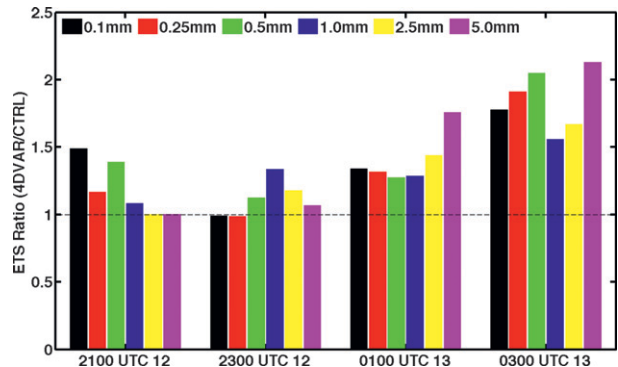


FIG. 14. The ratio of equitable threat scores (ETS) for 1-h accumulated precipitation between control and 4DVAR experiments with the threshold of 0.1, 0.25, 0.5, 1.0, 2.5, and 5.0 mm at 2100 UTC 12 Jun 2002, 2300 UTC 12 Jun 2002, 0100 UTC 13 Jun 2002, and 0300 UTC 13 Jun 2002.

c. Data impact: Conventional observations versus GLOW wind profiles

Figure 15 presents the simulated composite reflectivity at four different times from CONV (Figs. 15a–d) and BOTH (Figs. 15e–h) experiments, respectively. Compared to Fig. 11 (CTRL and 4DVAR) and Fig. 2 (lidar observations), the improvements of reflectivity simulation from assimilation of conventional data are very limited. Specifically, at 2100 UTC 12 June (end of the data assimilation Fig. 15a), the convections near the north of Oklahoma and Kansas border region (corresponding to Fig. 2a group B) are successfully simulated but the simulated reflectivity is a little overestimated compared to observations (Fig. 2a). Similar to the control run simulation, the locations of convective initiation for group A are not well simulated, the simulated reflectivity near the Texas and Oklahoma border is too intense (cf. the observations; Fig. 2a). During the following 6-h simulation, in CONV experiment, at 2300 UTC 12 June, the convective areas initiated from group A continue to grow up and intensify, while the convective elements initiated from group B intensify more quickly than CTRL; after that, the differences between CONV and the control run experiment decrease (Figs. 15c,d).

When both conventional observations and GLOW lidar wind profiles are assimilated (BOTH; Fig. 15e), the simulated reflectivity distribution is closer to the radar observations. The overestimated reflectivity near the Texas and Oklahoma border areas in CONV experiment has been improved after including the GLOW wind profiles into the assimilation. At 2300 UTC 12 June, a more intense reflectivity is simulated over the Texas and Oklahoma border area (corresponding to the convections initiated from group A). However, similar to CTRL, the convections near the northwest border of Oklahoma are

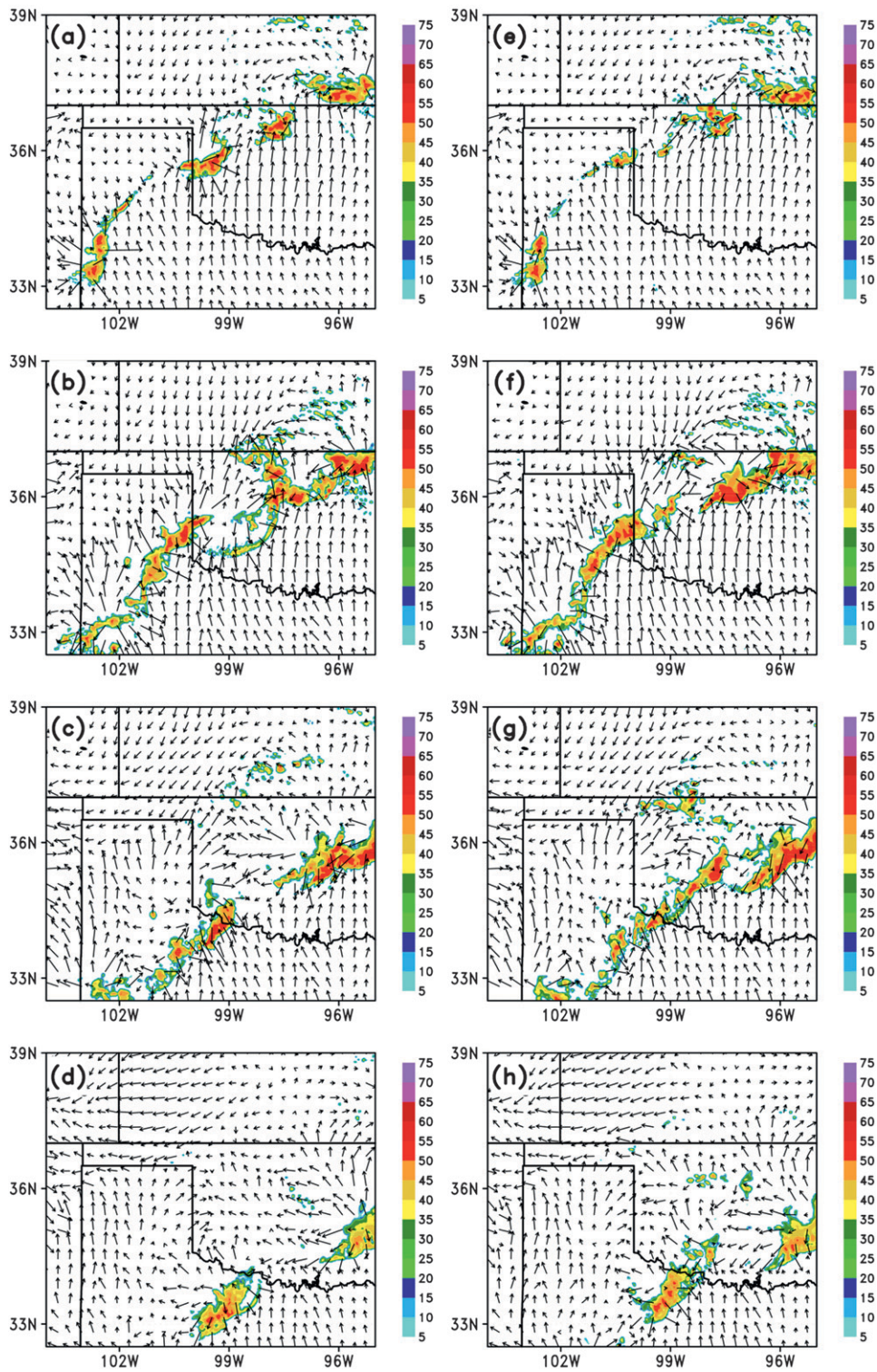


FIG. 15. As in Fig. 11, but for experiments (a)–(d) CONV and (e)–(h) BOTH.

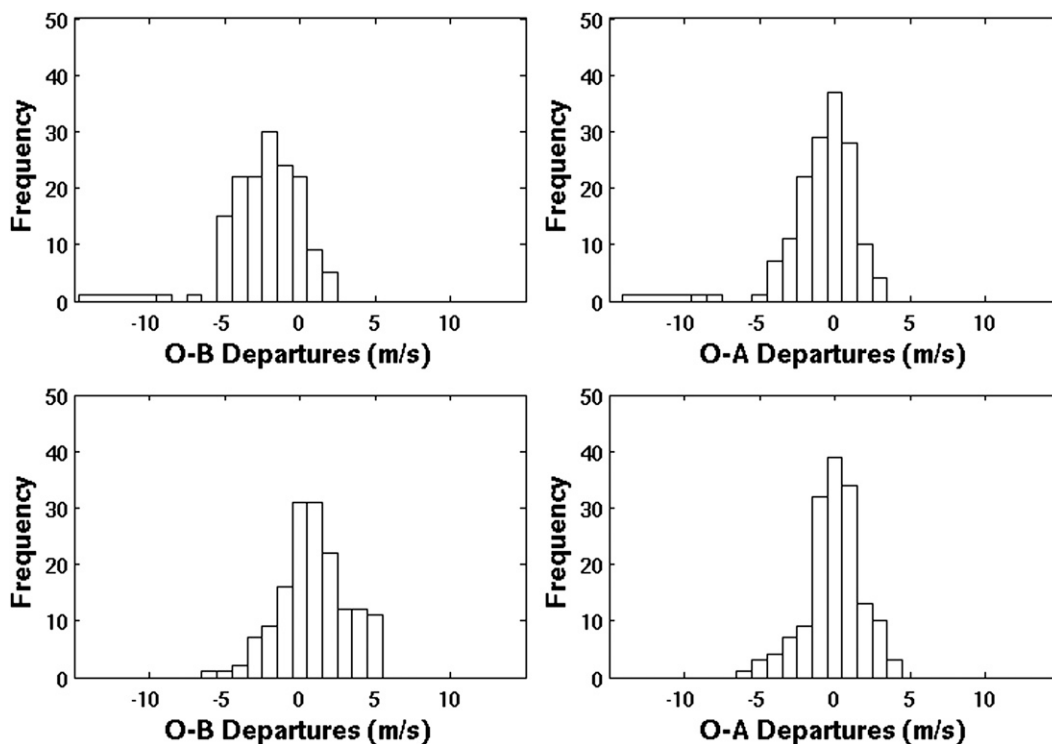


FIG. 16. As in Fig. 6, but that the results are calculated for the assimilation of conventional data experiment within the region that is marked by dashed lines in Fig. 4.

not well predicted. The main differences between CONV and BOTH experiments are found over the northwest border of Oklahoma area. The BOTH predicts weaker convective elements (cf. Fig. 2c), which were missing in the CTRL (Fig. 12c) and CONV (Fig. 15c) experiments, implying the improvement is due to the inclusion of GLOW wind observations during the assimilation.

Overall, the numerical results from both CONV and BOTH are not compatible with the 4DVAR experiment with the assimilation of GLOW wind profiles only. Compared with the analysis increment from 4DVAR (e.g., Fig. 5) the analysis increments for wind components, temperature, and moisture from CONV (figures not shown) are too small over the region with convective group A (Fig. 2). Figure 16 further confirms the possible reason of the small impact of the conventional data by showing the statistic differences between conventional observations and the background wind field over the square box in Fig. 4. It is clear that the differences between the conventional observations and background are too small, leaving very little room for additional improvements. When both conventional data and GLOW wind profiles are assimilated, these conventional data act as an observational constraint, thus preventing the GLOW data from imposing a strong influence on the area that has conventional data (mostly surface data) coverage.

6. Conclusions

The importance of moisture fields in mesoscale convective initiations has been well recognized and studied extensively during IHOP_2002, while the influence of the high temporal and vertical resolution wind profile measurements on numerical simulations and predictions of mesoscale convections have not been paid much attention. In this study, the impact of high vertical and temporal wind profiles on the short-range simulation and prediction of mesoscale convective events is investigated through the 4DVAR data assimilation using the WRF model. Convections that occurred on 12–13 June 2002 over the region from the Kansas and Oklahoma border to the Texas Panhandle during the IHOP_2002 are studied. Results indicate that the high vertical and temporal resolution wind observations have a significant influence on the convective initiation and evolution. The assimilation of high-resolution wind information has resulted in redistributions in the wind, temperature, and moisture fields and results in the more realistic simulations of the convection systems. Even though only wind information was assimilated, the temperature and moisture fields were also adjusted. Compared with the observations, the simulated precipitation evolutions of the mesoscale convective system in 4DVAR are more realistic than that from the control simulation.

The predicted precipitation locations are in agreement with the observed precipitation locations with enhanced skill of QPF in most of cases.

Though the wind profile measurements assimilated in the 4DVAR experiment come from a single station, analysis increments have been obtained with a spatial distribution (Fig. 5). These results from the 4DVAR experiment clearly demonstrated its ability in accomplishing the time and space information conversion, a concept proposed by Fujita (1963) many years ago. Therefore, the positive impact of 4DVAR assimilation of multitime data over a single station on the mesoscale prediction in this study also presents a successful execution of the traditional time-to-space conversion technique (Fujita 1963).

The positive impact of wind profile measurements on the numerical simulation of mesoscale systems from this study agree with the conclusion from a recent study by Pu et al. (2010), in which the airborne Doppler wind lidar measured wind profiles have a great impact on the numerical simulation of a tropical cyclone.

However, when assimilating conventional observations (surface and radiosonde data) with GLOW wind profiles, the results are not compatible with those from only assimilating the GLOW wind profiles, showing a negative impact of conventional data in integrated data assimilation. This result, however, is opposite to the conclusion from Pu et al. (2010), in which the integrated data assimilation showed more promising results. The main reason for the small impact on this specific case could be attributed to the better coverage of these conventional data as they provide constraints during the data assimilation, thus, adding additional data (GLOW wind data) from a single station could not influence the analysis in the same areas. In Pu et al. (2010), the conventional data are generally sparse over the ocean. Since lots of conventional data used in this study are surface data, the results might imply that high temporal and spatial resolution profile data are necessary in the future in order to impose a reasonable influence to the whole boundary layer analysis. Future work will be conducted to draw more robust conclusions regarding the role of the possible atmospheric wind-profiling network in the initiation and evolution of mesoscale convective systems. In addition, as a recent study by Zhang et al. (2011) found that the ensemble Kalman filter (EnKF) method has advantages over the 4DVAR method in assimilating conventional observations (especially moisture data), a future study will also be performed to evaluate the more efficient data assimilation method for integrated data assimilation.

Acknowledgments. The authors thank Drs. Bruce Gentry and Belay Demoz at NASA GSFC for providing GLOW lidar wind data and valuable discussion on the

data quality. They are also grateful to NCAR WRF model development group. Specifically, they would like to thank Drs. Xiang-Yu Hans Huang and Xin Zhang for making the 4DVAR system available. The computer time for this study is provided by the Center for High Performance Computing (CHPC) at the University of Utah and NASA high-end computing systems. This study is supported by NASA Grant NNX08AH88G, NSF Grant 08339856, and the Office of Science (BER), U.S. Department of Energy. The review comments from three anonymous reviewers and Prof. Fuqing Zhang, from The Pennsylvania State University, were very helpful in improving this manuscript.

REFERENCES

- Barker, D. M., W. Huang, Y. R. Guo, A. J. Bourgeois, and Q. N. Xiao, 2004: A three-dimensional data assimilation system for use with MM5: Implementation and initial results. *Mon. Wea. Rev.*, **132**, 897–914.
- Chen, F., and J. Dudhia, 2001: Coupling an advanced land-surface/hydrology model with the Penn State/NCAR MM5 modeling system. Part I: Model description and implementation. *Mon. Wea. Rev.*, **129**, 569–585.
- Chen, S.-H., and W.-Y. Sun, 2002: A one-dimensional time dependent cloud model. *J. Meteor. Soc. Japan*, **80**, 99–118.
- Childs, P. P., A. L. Qureshi, S. Raman, K. Alapaty, R. Ellis, R. Boyles, and D. Niyogi, 2006: Simulation of convective initiation during IHOP_2002 using the Flux-Adjusting Surface Data Assimilation System (FASDAS). *Mon. Wea. Rev.*, **134**, 134–148.
- Courtier, P., J.-N. Thépaut, and A. Hollingsworth, 1994: A strategy for operational implementation of 4D-Var, using an incremental approach. *Quart. J. Roy. Meteor. Soc.*, **120**, 1367–1387.
- Crook, N. A., and J. Sun, 2002: Assimilating radar, surface and profiler data for the Sydney 2000 forecast demonstration project. *J. Atmos. Oceanic Technol.*, **19**, 888–898.
- Dudhia, J., 1989: Numerical study of convection observed during the winter monsoon experiment using a mesoscale two-dimensional model. *J. Atmos. Sci.*, **46**, 3077–3107.
- Fritsch, J. M., and R. E. Carbone, 2004: Improving quantitative precipitation forecasts in the warm season: A USWRP research and development strategy. *Bull. Amer. Meteor. Soc.*, **85**, 955–965.
- Fujita, T., 1963: Analytical mesometeorology: A review. *Severe Local Storms, Meteor. Monogr.*, No. 27, Amer. Meteor. Soc., 77–128.
- Gentry, B. M., and H.-L. Chen, 2003: Tropospheric wind measurements obtained with the Goddard Lidar Observatory for Winds (GLOW): Validation and performance. *Lidar Remote Sensing for Industry and Environment Monitoring II*, U. N. Singh, Ed., International Society for Optical Engineering (SPIE Proceedings, Vol. 4484), 74–81.
- Hong, S.-Y., and H.-L. Pan, 1996: Nonlocal boundary layer vertical diffusion in a medium-range forecast model. *Mon. Wea. Rev.*, **124**, 2322–2339.
- Huang, X.-Y., and Coauthors, 2009: Four-dimensional variational data assimilation for WRF: Formulation and preliminary results. *Mon. Wea. Rev.*, **137**, 299–314.
- Kain, J. S., and J. M. Fritsch, 1993: The role of the convective “trigger function” in numerical prediction of mesoscale convective systems. *Meteor. Atmos. Phys.*, **49**, 93–106.
- Lee, B. D., R. D. Farley, and M. R. Hjelmfelt, 1991: A numerical case study of convection initiation along colliding convergence

- boundaries in northeast Colorado. *J. Atmos. Sci.*, **48**, 2350–2366.
- LeMone, M. A., E. Zipser, and S. B. Trier, 1998: The role of environmental shear and thermodynamic conditions in determining the structure and evolution of mesoscale convective systems during TOGA COARE. *J. Atmos. Sci.*, **55**, 3493–3518.
- Liu, H., and M. Xue, 2008: Prediction of convective initiation and storm evolution on 12 June 2002 during IHOP_2002. Part I: Control simulation and sensitivity experiments. *Mon. Wea. Rev.*, **136**, 2261–2282.
- Lorenc, A. C., 2003: Modelling of error covariances by four-dimensional variational data assimilation. *Quart. J. Roy. Meteor. Soc.*, **129**, 3167–3182.
- Mlawer, E. J., S. J. Taubman, P. D. Brown, M. J. Iacono, and S. A. Clough, 1997: Radiative transfer for inhomogeneous atmosphere: RRTM, a validated correlated-k model for the longwave. *J. Geophys. Res.*, **102**, 16 663–16 682.
- Parrish, D. F., and J. C. Derber, 1992: The National Meteorological Center's spectral statistical interpolation analysis system. *Mon. Wea. Rev.*, **120**, 1747–1763.
- Pu, Z., L. Zhang, and G. D. Emmitt, 2010: Impact of airborne Doppler wind lidar data on numerical simulation of a tropical cyclone. *Geophys. Res. Lett.*, **37**, L05801, doi:10.1029/2009GL041765.
- Skamarock, W. C., J. B. Klemp, J. Dudhia, D. O. Gill, D. M. Barker, W. Wang, and J. G. Powers, 2005: A description of the advanced research WRF Version 2. NCAR Tech. Note NCAR/TN-468+STR, 88 pp.
- Stauffer, D., and N. L. Seaman, 1990: Use of four-dimensional data assimilation in a limited-area mesoscale model. Part I: Experiments with synoptic-scale. *Mon. Wea. Rev.*, **118**, 1250–1277.
- Sun, J., and N. A. Crook, 2001: Real-time low-level wind and temperature analysis using single WSR-88D data. *Weather Forecasting*, **16**, 117–132.
- Veerse, F., and J. N. Thépaut, 1998: Multiple-truncation incremental approach for four-dimensional variational data assimilation. *Quart. J. Roy. Meteor. Soc.*, **124**, 1889–1908.
- Wakimoto, R. M., H. V. Murphey, and R. G. Fovell, 2004: Mantle echoes associated with deep convection: Observations and numerical simulations. *Mon. Wea. Rev.*, **132**, 1701–1720.
- Weckwerth, T. M., and Coauthors, 2004: An overview of the International H₂O Project (IHOP_2002) and some preliminary highlights. *Bull. Amer. Meteor. Soc.*, **85**, 253–277.
- , H. V. Murphey, C. Flamant, J. Goldstein, and C. R. Pettet, 2008: An observational study of convective initiation on 12 June 2002 during IHOP_2002. *Mon. Wea. Rev.*, **136**, 2283–2304.
- Wilks, D. S., 1995: *Statistical Methods in Atmospheric Sciences*. Academic Press, 467 pp.
- Wulfmeyer, V., H.-S. Bauer, M. Grzeschik, A. Behrendt, F. Vandenberghe, E. V. Browell, S. Ismail, and R. A. Ferrare, 2006: Four-dimensional variational assimilation of water vapor differential absorption lidar data: The first cast study within IHOP_2002. *Mon. Wea. Rev.*, **134**, 209–230.
- Xiao, Q.-N., and J. Sun, 2007: Multi-radar data assimilation and short-range quantitative precipitation forecasting of a squall line observed during IHOP_2002. *Mon. Wea. Rev.*, **135**, 3381–3404.
- Xue, M., and W. J. Martin, 2006: A high-resolution modeling study of the 24 May 2002 case during IHOP. Part I: Numerical simulation and general evolution of the dryline and convection. *Mon. Wea. Rev.*, **134**, 149–171.
- Zängl, G., 2004: The sensitivity of simulated orographic precipitation to model components other than cloud microphysics. *Quart. J. Roy. Meteor. Soc.*, **130**, 1857–1875.
- Zhang, F., A. Odins, and J. W. Nielsen-Gammon, 2006: Mesoscale predictability of an extreme warm-season rainfall event. *Weather Forecasting*, **21**, 149–166.
- Zhang, M., F. Zhang, X.-Y. Huang, and X. Zhang, 2011: Intercomparison of an ensemble Kalman filter with three- and four dimensional variational data assimilation methods in a limited-area model during the month of June 2003. *Mon. Wea. Rev.*, **139**, 566–572.